NACA RM E52K18

NACA

RESEARCH MEMORANDUM

INVESTIGATION AT SUPERSONIC SPEEDS OF AN INLET EMPLOYING CONICAL FLOW SEPARATION FROM A PROBE AHEAD OF A BLUNT BODY

By Donald P. Hearth and Gerald C. Gorton

Lewis Flight Propulsion Laboratory
Cleveland, Ohio

NATIONAL ADVISORY COMMITTEE
FOR AERONAUTICS
WASHINGTON

January 19, 1953
Declassified November 8, 1957

NATIONAL ADVISORY COMMITTEE FOR AERONAUTICS

RESEARCH MEMORANDUM

INVESTIGATION AT SUPERSONIC SPEEDS OF AN INLET EMPLOYING CONICAL FLOW SEPARATION FROM A PROBE AHEAD OF A BLUNT BODY

By Donald P. Hearth and Gerald C. Gorton

SUMMARY

An investigation was made in the Lewis 8- by 6-foot supersonic wind tunnel on an inlet employing conical flow separation from a probe extending upstream from a hemispherical-nosed centerbody. Data were obtained at free-stream Mach numbers from 1.6 to 2.0 and angles of attack from 0° to 9°.

Pressure-recovery and drag characteristics for the inlet were very nearly comparable with those for a conical-spike inlet at zero angle of attack and design Mach number of 2.0, but compared less favorably at Mach numbers below 2.0.

A large reduction in pressure recovery and mass flow was obtained at angle of attack. However, an investigation on the use of probes offset from the inlet center line indicated that the angle-of-attack performance could be appreciably improved if the probe were alined with the stream direction.

INTRODUCTION

When a probe or rod is extended sufficiently forward of a blunt-nosed body in a supersonic stream, flow separation occurs from the probe (references 1 to 8). This phenomenon occurs because of the inability of the boundary layer on the probe to withstand the large static-pressure rise associated with the detached shock caused by the blunt body. Various investigations (references 1 to 5) have been conducted applying this form of flow separation as a means of reducing the drag of blunt-nosed bodies at supersonic speeds. Application of this separation phenomenon to supersonic inlets has been initiated (reference 6) by utilizing the separated-flow-region boundary as the compression surface in place of the usual solid cone. Because of the spherical shape of the blunt body, such an inlet would be more desirable as a housing for a radar homing system than a conical-spike inlet.

In order to evaluate this type of inlet, an investigation was conducted in the NACA Lewis 8- by 6-foot supersonic wind tunnel on an inlet consisting of a hemispherical-nosed centerbody with a probe projected upstream. Pressure-recovery, drag, and mass-flow characteristics are presented for Mach numbers from 1.6 to 2.0 and angles of attack to 9°. The Reynolds number, based on inlet diameter, was approximately 2.07×10^{6}. Data for a conical inlet installed on the same model (reference 9) are included for comparison.

SYMBOLS

The following symbols are used in this report:

A	area, sq ft
C_D	external-drag coefficient D/q_0A_m
D	drag force, lb
L	length of probe, in.
M	Mach number
m	mass flow, slugs/sec
m/m_0	mass-flow ratio
P	total pressure, lb/sq ft
p	static pressure, lb/sq ft
q	dynamic pressure, $\gamma pM^2/2$, lb/sq ft
R	radius of hemispherical nose, in.
α	angle of attack, deg
γ	ratio of specific heats for air

Subscripts:

0	free stream
2	station 1/2 inch upstream of honeycomb
m	maximum

APPARATUS AND PROCEDURE

The separation inlet configuration, as installed on an 8-inch cold-flow ram-jet engine, is shown schematically in figure 1. With the exception of the cowl, the outer shell was identical to that used on the model reported in reference 9. The internal cowl-lip angle was so chosen that it would be alined with the flow at $M_0 = 2.0$ if the same type of shock structure observed in reference 6 was obtained. Details of the hemispherical-nosed centerbody, the variable-length straight probe, and the cowl are also shown in figure 1. The included angle of the probe tip was 30°. Internal and external coordinates for the cowl are presented in table I.

A photograph of the separation inlet as installed in the 8- by 6-foot supersonic wind tunnel is shown in figure 2 and the notations used in the data presentation are illustrated in figure 3. From a station 1.8 inlet diameters downstream of the cowl lip to the plane of survey (station 3), the subsonic diffuser-area variation was identical to that of inlet A of reference 9 and was similar to that from the cowl lip to the 1.8 station. This variation is presented in figure 4.

Mass-flow ratio is presented as the ratio of the actual mass flow through the inlet to that through a free-stream tube defined by the cowl-inlet area. Variation of mass flow was accomplished by means of a movable plug at the exit of the model. Actual mass flow through the inlet was computed for choking at the control-plug minimum area by the use of an average static pressure measured at the plane of survey (station 3) in conjunction with isentropic-flow relations. The honeycomb, shown in figure 1, was used to minimize the angularity of the flow at the plane of survey and to obtain smooth air flow prior to the exit plug.

Total-pressure recovery is presented as the ratio of the total pressure ahead of the honeycomb (station 2) to the free-stream total pressure. By use of measured static pressures at stations 2 and 3, the total pressure ahead of the honeycomb was calculated from continuity relations, assuming that an adiabatic process existed between these two stations.

Drag data were computed from the axial-force data measured by a three-component strain-gage balance and are presented in coefficient form, based on the maximum external cross-sectional area of the model (0.360 sq ft). Angle-of-attack correction was determined from a static calibration of the support-sting deflection resulting from various combinations of balance normal and moment forces.

A dynamic pressure pickup, located slightly downstream of the plane of survey, was used to determine inlet instability. In addition, flash and high-speed schlieren photographs were obtained.

RESULTS AND DISCUSSION

In order to optimize the inlet at a Mach number of 2.0 and zero angle of attack, a preliminary investigation was conducted in which the probe length and the relative cowl positions at these conditions were varied. With the cowl in its original position (cowl position A, fig. 3(a)), maximum-pressure-recovery points were obtained at various probe lengths. These data, as presented in figure 5(a), indicate the same trend of maximum pressure recovery and movement of the separation origin reported in reference 6. For short probe lengths, the flow separated from the conical portion of the probe, that is, from the probe tip, and the maximum pressure recovery increased as the probe was extended, reaching a peak value of 0.85 at a probe length parameter value (L/R) of 1.27. This value of L/R for the highest maximum pressure recovery agrees very closely with that reported in reference 6. For further extensions of the probe, the flow continued to separate from the probe tip and the maximum pressure recovery decreased, until a critical L/R value of about 2.80 was reached; at this value, the flow separation "jumped" and began occurring from the cylindrical portion of the probe. At this point the maximum pressure recovery increased to about 0.80 and remained approximately constant for further extensions of the probe. It was found that the two types of separation (that is, separation from the probe tip and from the probe surface) approximately followed the trends of Reynolds number and pressure rise across the accompanying shock wave for laminar and turbulent separation as reported in reference 10. A full range of data was obtained for the probe setting which yielded the highest maximum pressure recovery and it was found that this configuration was spilling 8 percent of the mass flow at critical operation.

To more nearly capture a full free-stream tube at critical operation, the spacers (fig. 1) were adjusted so that the cowl was in position B (fig. 3(a)). With the cowl in this position, maximum-pressure-recovery points were obtained at various probe lengths as before. These data, as presented in figure 5(b), show the same trend as obtained with cowl position A. The highest maximum pressure recovery again occurred at an L/R value of 1.27, but the peak value for this cowl position was reduced to 0.83. However, the critical mass-flow ratio at this L/R value was increased to almost unity. As indicated in the figure, there existed a hysteresis effect at the transition point where the origin of the separation "jumped". This effect, which appears to be of the same nature as that reported in references 3 and 7, was also noted for cowl position A.

Schlieren photographs obtained at maximum-pressure-recovery points for both cowl positions are shown in figure 6. At an L/R value of 1.27 (fig. 6(a)), a second oblique shock was present with the cowl in position A. This second oblique shock, which was present for all L/R

values, appears to be of the same nature as that reported and discussed in references 4 to 6. When the cowl was moved forward to position B, the second oblique shock was again present at critical operation with flow separation from the probe tip. However, at the maximum-pressure-recovery point, the second oblique shock was eliminated; this can easily be seen by a comparison of figures 6(a) and 6(b). Undoubtedly the elimination of the second oblique shock was partly the cause for the lower level of pressure recovery shown in figure 5(b) (other causes being changes in effective cone angle, internal geometry, and so forth). Presumably, the advanced position of the normal shock on the centerbody induced a higher pressure in the dead-air region thereby increasing the effective cone angle and causing the boundary of the separated flow to strike the centerbody tangentially; the flow deflection which produced the second oblique shock was thus eliminated. Another possible explanation is that the normal shock may have been moved sufficiently forward to extend a subsonic-flow field into the region where a deflection of the separated flow boundary is needed, thereby eliminating the second oblique shock.

Presented in figure 6(c) is a typical schlieren photograph of separation on the probe surface. Measurements of the shock configuration indicated very nearly conical flow. The half-angle of the dead-air region at the highest maximum-pressure-recovery condition for cowl position B was approximately 27° which is very close to the optimum cone-half-angle for a Mach number of 2.0.

Variation of pressure recovery and drag coefficient with mass-flow ratio at a Mach number of 2.0 and zero angle of attack for the two cowl positions at the optimum probe lengths is presented in figure 7. Also included are data obtained for a conical inlet installed on the same model (inlet A of reference 9). The relative forward movement of the cowl decreased the maximum pressure recovery from 0.85 to 0.83 and the critical pressure recovery from 0.83 to 0.81. However, the movement of the cowl caused an increase in the critical mass-flow ratio from 0.92 to 0.99. Since the configuration with the cowl in position B was able to capture very nearly a full free-stream tube at critical operation, this cowl position was considered the optimum one.

The pressure-recovery and mass-flow characteristics for the optimized separation inlet appear to be similar to those for the conical inlet, except that the absolute values of the pressure recovery are somewhat lower as can be seen from figure 7. Pressure recoveries for the conical and the separation inlets at critical operation were 0.83 and 0.81, respectively, while the maximum pressure recoveries were 0.85 and 0.83, respectively. Comparable stability characteristics were noted for the two inlets. The drag coefficient for the separation inlet was slightly higher than for the conical inlet; the values at critical operation being 0.12 and 0.10, respectively. However, the

higher drag may be attributed to the larger external cowl-lip angle of 27° for the separation inlet as compared with the 12° angle for the conical inlet. Cowl pressure-drag coefficients were calculated for the separation and the conical inlets by linearized potential theory and were found to be 0.051 and 0.035, respectively. These values of cowl pressure drag indicate that the total drag of the separation inlet might be expected to equal that of the conical inlet if similar cowl-lip angles are employed.

It also appears from figure 7 that the drag coefficient of the optimized separation inlet increased at a lower rate than the drag coefficient of the conical inlet for the same amount of mass-flow spillage. Since the value of the oblique shock angle of the optimized separation inlet increased with decreasing mass-flow ratio, it might be expected that the mass-flow spillage of this inlet consisted of some supersonic spillage, as well as the usual subsonic spillage. Because of the lower additive drag associated with supersonic spillage (reference 11), a lower slope of the drag curve might be expected.

Variation of total-pressure recovery and drag coefficient with mass-flow ratio for the optimum length straight probe for cowl position B over the ranges of Mach numbers and angles of attack investigated are presented in figure 8. These data are cross plotted in figure 9.

The effect of Mach number on the separation-inlet performance at zero angle of attack, as compared with the performance of a conical inlet, is shown in figure 9(a) for critical operation and figure 9(b) for operation at maximum pressure recovery. As shown in the figure, the critical pressure recovery of the separation inlet compared less favorably with that of the conical inlet at Mach numbers lower than 2.0. (Note: at a Mach number of 1.6, the values are 0.86 and 0.93, respectively.) The angle of the dead-air region (effective cone angle) increased slightly with decreasing Mach number, thereby causing more low-energy air to enter the inlet. This may account, in part, for the relatively poorer pressure recovery of the separation inlet at the lower Mach numbers. In addition, observations indicated that the boundary of the dead-air region was more irregular as the Mach number was decreased.

In addition to the lower pressure recovery, the separation inlet exhibited a large decrease in the critical mass-flow ratio at Mach numbers below 2.0. As can be seen from figure 9(a), this decrease in mass-flow ratio is greater than for a conical inlet and is probably due, in part, to the increase in effective cone angle as the Mach number is decreased. No gain in performance could be attained for Mach numbers less than 2.0 by varying the probe length from the L/R

value of 1.27. The difference in drag noted previously at a Mach number of 2.0 appeared to be constant over the range of Mach numbers investigated. Schlieren photographs at zero angle of attack and Mach numbers of 2.0 and 1.8 are presented in figure 10 for the maximum-pressure-recovery condition.

As indicated in figure 8, there was a large loss in performance at angle of attack similar to that reported in reference 6. It was suggested in reference 6 that the performance at angle of attack might be improved by alining the probe with the air stream. To evaluate this recommendation, two additional probes, offset 5° and 10° from the center line of the model, were investigated over the same range of variables as for the straight probe. Data are presented in figures 11 and 12 for the 5° and 10° probes, respectively. These data, as well as the original data, are cross-plotted in figure 13.

The effect of angle of attack on the performance of the various probes at a Mach number of 2.0 is summarized in figure 13(a) for critical operation and in figure 13(b) for operation at maximum pressure recovery. The configuration with the straight probe suffered a large loss in performance as the inlet was raised to angles of attack. The reason for this large loss in performance can be seen from the schlieren photographs presented in figures 14(a) to 14(c). Because of the tendency of the separated flow region to aline itself with the stream direction, a large quantity of the low-energy separated air entered the upper half of the inlet and a strong shock wave formed over the lower half of the inlet as the angle of attack was increased.

Results for the offset probes, shown in figure 13, indicate a marked gain in performance over the straight probe at the angles of attack for which the probe was nearly alined with the flow. For example, an increase in critical pressure recovery from 0.74 to 0.78 was obtained at a 5° angle of attack. It can be seen from figures 14(d) and 14(e) that the 5° probe at a 5° angle of attack and the 10° probe at a 9° angle of attack cause the separated flow region to be very nearly tangent to the blunt body; thereby the poor flow field associated with the straight probe at the same angles of attack (figs. 14(b) and 14(c)) is avoided. It was noted that the inlet with the offset probes had stability characteristics comparable with those of the inlet with the straight probe.

The expected performance of a separation inlet, consisting of a probe which would be alined with the stream direction at all angles of attack, is illustrated by the dashed curves in figure 13, which were obtained by connecting the data for the alined conditions. As indicated, the performance of this type inlet would be very nearly comparable with that of a fixed conical inlet at angles of attack. However, the results of this investigation indicate that the pressure

recovery of a conical-spike inlet at angle of attack may also be improved by alining the center line of the cone with the stream direction.

SUMMARY OF RESULTS

The following results were obtained from the investigation of an inlet utilizing flow separation from a probe extending upstream of a hemispherical-nosed centerbody.

1. Pressure-recovery, stability, and drag characteristics for the inlet were very nearly comparable with those for a conical-spike inlet at zero angle of attack and Mach number of 2.0, but compared less favorably with those for a conical-spike inlet at Mach numbers below 2.0.

2. A large loss in pressure recovery and mass flow at angle of attack was noted for the straight-probe configuration. However, results of an investigation of two other probes, offset 5° and 10° from the inlet center line, indicated that a configuration which alined the probe with the stream direction would have greatly improved angle-of-attack performance.

3. For the configuration which yielded a critical mass-flow ratio of nearly unity, a one-oblique-shock system was obtained at the maximum pressure-recovery condition. However, a two-oblique-shock system, with resulting higher pressure recovery, could be obtained at the expense of spilling 8 percent of the critical mass flow.

Lewis Flight Propulsion Laboratory
National Advisory Committee for Aeronautics
Cleveland, Ohio

REFERENCES

1. Alexander, Sidney R., and Katz, Ellis: Flight Tests to Determine the Effect of Length of a Conical Windshield on the Drag of a Bluff Body at Supersonic Speeds. NACA RM L6J16a, 1947.

2. Alexander, Sidney R.: Flight Investigations at Low Supersonic Speeds to Determine the Effectiveness of Cones and a Wedge in Reducing the Drag of Round-Nose Bodies and Airfoils. NACA RM L8L07a, 1949.

3. Beastall, D., and Turner, J.: The Effect of a Spike Protruding in Front of a Bluff Body at Supersonic Speeds. Tech. Note AERO. 2137, British R.A.E., Jan. 1952.

4. Jones, Jim J.: Flow Separation from Rods Ahead of Blunt Noses at Mach Number 2.72. NACA RM L52E05a, 1952.

5. Moeckel, W. E.: Flow Separation Ahead of a Blunt Axially Symmetric Body at Mach Numbers 1.76 to 2.10. NACA RM E51I25, 1951.

6. Moeckel, W. E., and Evans, P. J. Jr.: Preliminary Investigation of Use of Conical Flow Separation for Efficient Supersonic Diffusion. NACA RM E51J08, 1951.

7. Lukasiewicz, J.: Conical Flow as Result of Shock and Boundary Layer Interaction on a Probe. Tech. Note AERO. 1968, British R.A.E., Sept. 1948.

8. Mair, W. A.: Experiments on Separation of Boundary Layers on Probes in Front of Blunt-Nosed Bodies in a Supersonic Air Stream. Phil. Mag., vol. 43, no. 342, July 1952, pp. 695-716.

9. Beke, Andrew, and Allen, J. L.: Force and Pressure-Recovery Characteristics of a Conical-Type Nose Inlet Operating at Mach Numbers of 1.6 to 2.0 and at Angles of Attack to 9°. NACA RM E52I30, 1952.

10. Donaldson, Coleman du P., and Lange, Roy H.: Study of the Pressure Rise Across Shock Waves Required to Separate Laminar and Turbulent Boundary Layers. NACA TN 2770, 1952. (Supersedes NACA RM L52C21.)

11. Sibulkin, Merwin: Theoretical and Experimental Investigation of Additive Drag. NACA RM E51B13, 1951.

TABLE I. - COWL COORDINATES FOR SEPARATION INLET

Station distance from cowl lip (in.)	Internal diameter (in.)	External diameter (in.)
0	5.532	5.532
.10	5.600	5.644
.20	5.674	5.746
.30	5.732	5.838
.40	5.788	5.918
.60	5.878	6.046
.80	5.950	6.148
1.00	6.010	6.232
1.50	6.120	6.370
2.00	6.200	6.450
2.50	6.268	6.518
3.00	6.326	6.576
3.50	6.376	6.626
4.00	6.418	6.668
4.50	6.456	6.706
5.00	6.492	6.742
7.50	6.625	6.870
10.00	6.750	7.000
20.00	7.200	7.460
32.14	7.875	8.125
56.125	7.875	8.125

NACA

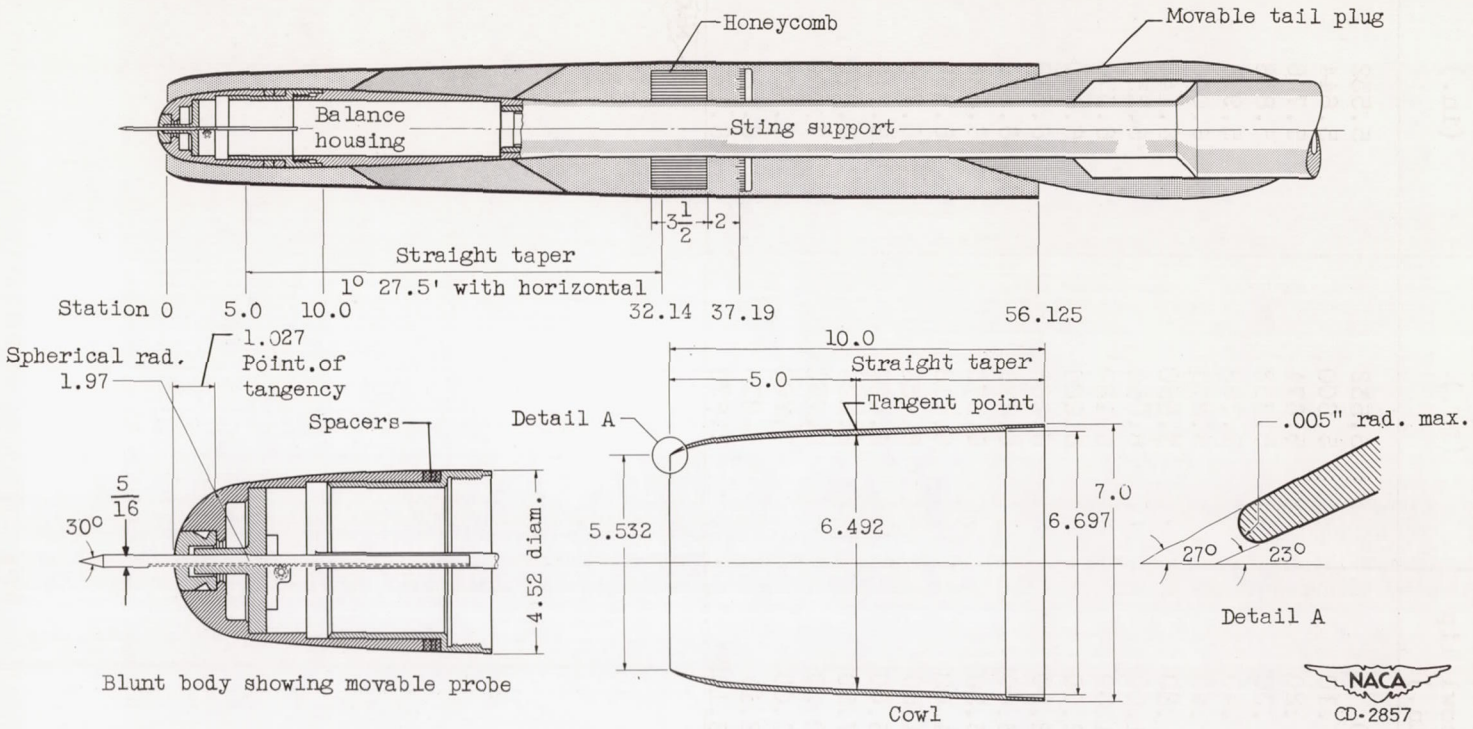

Figure 1. - Schematic diagram of 8-inch ram-jet engine showing principal dimensions of model and details of separation inlet. (All dimensions in inches.)

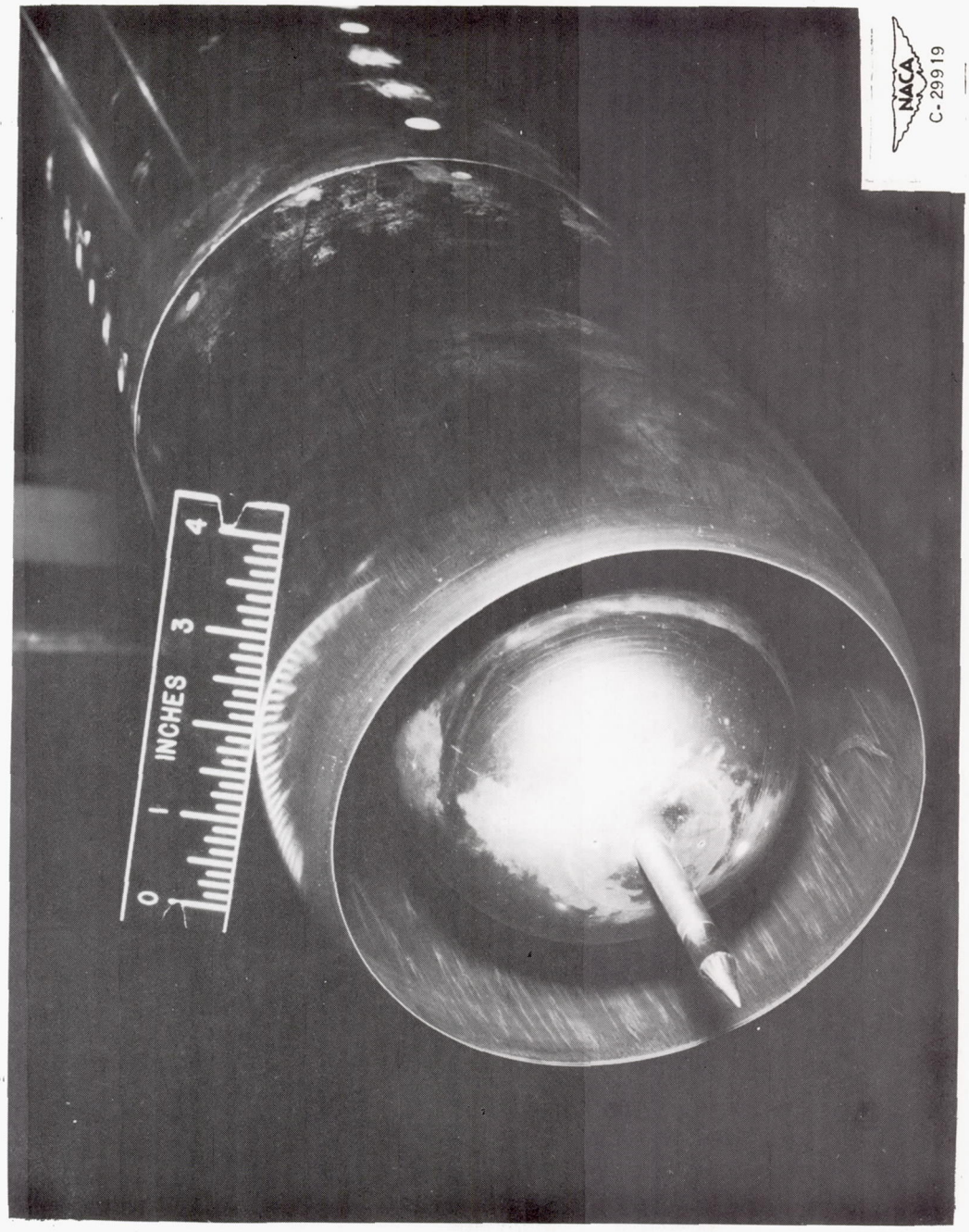

Figure 2. - Three-quarter front view of separation inlet.

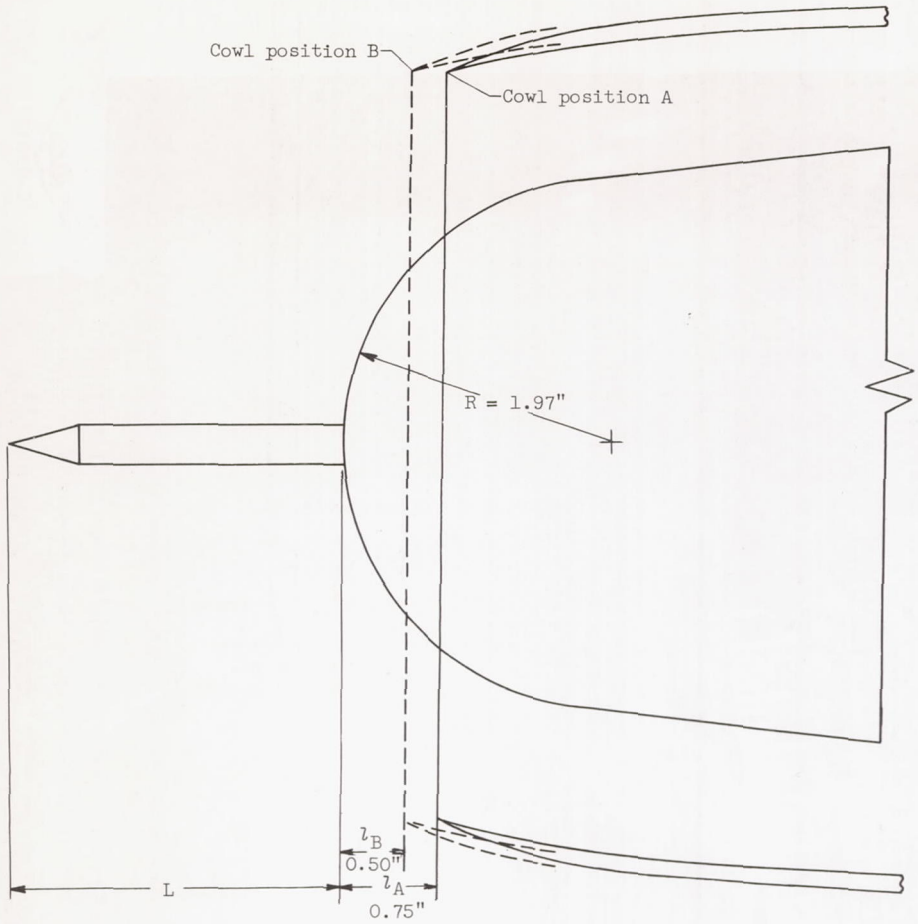

(a) Probe length and cowl position parameters.

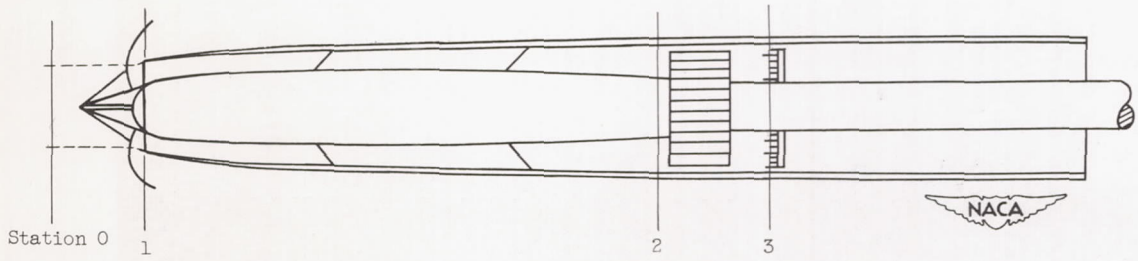

(b) Position of stations.

Figure 3. - Notation for separation inlet.

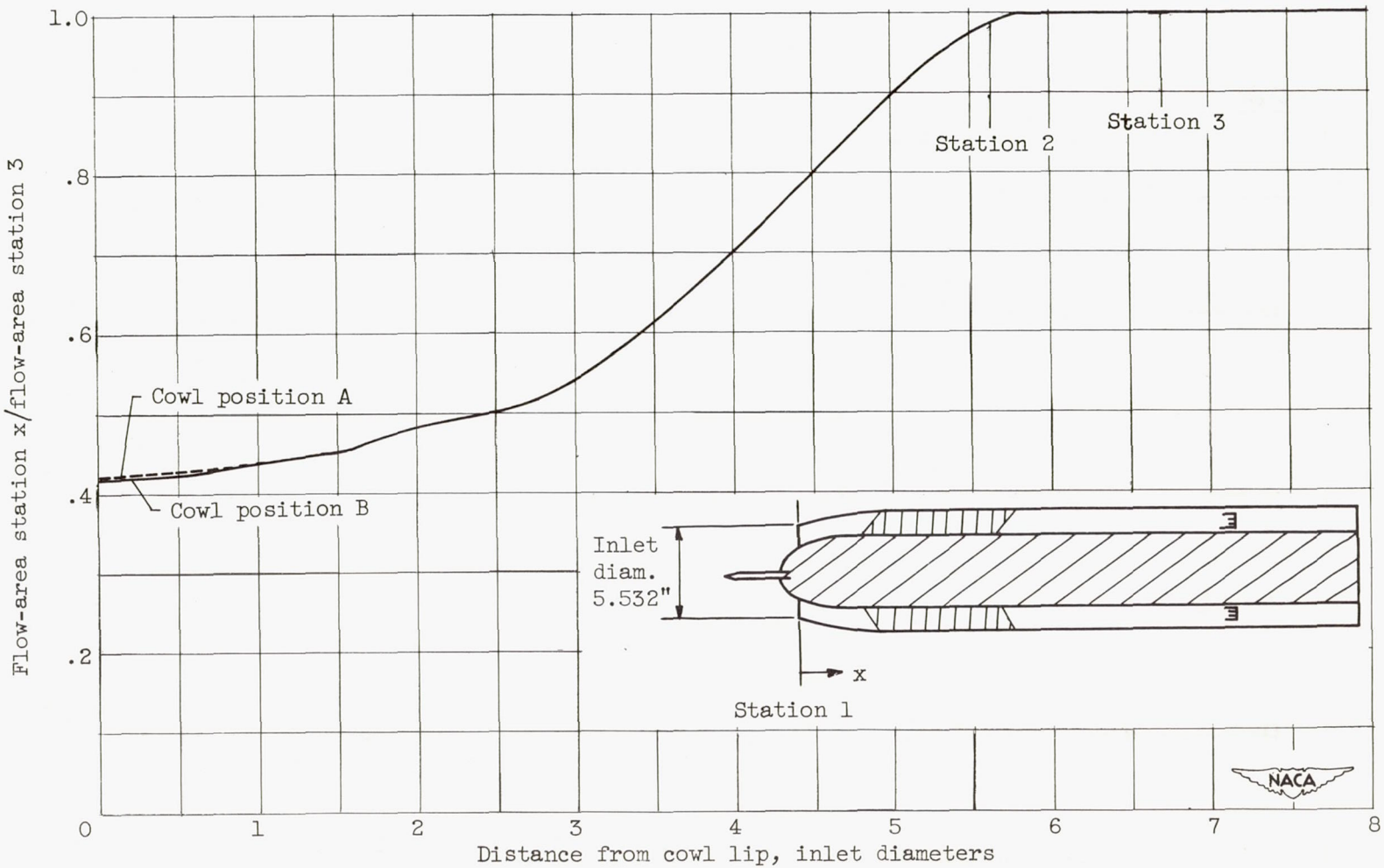

Figure 4. - Diffuser-area variation.

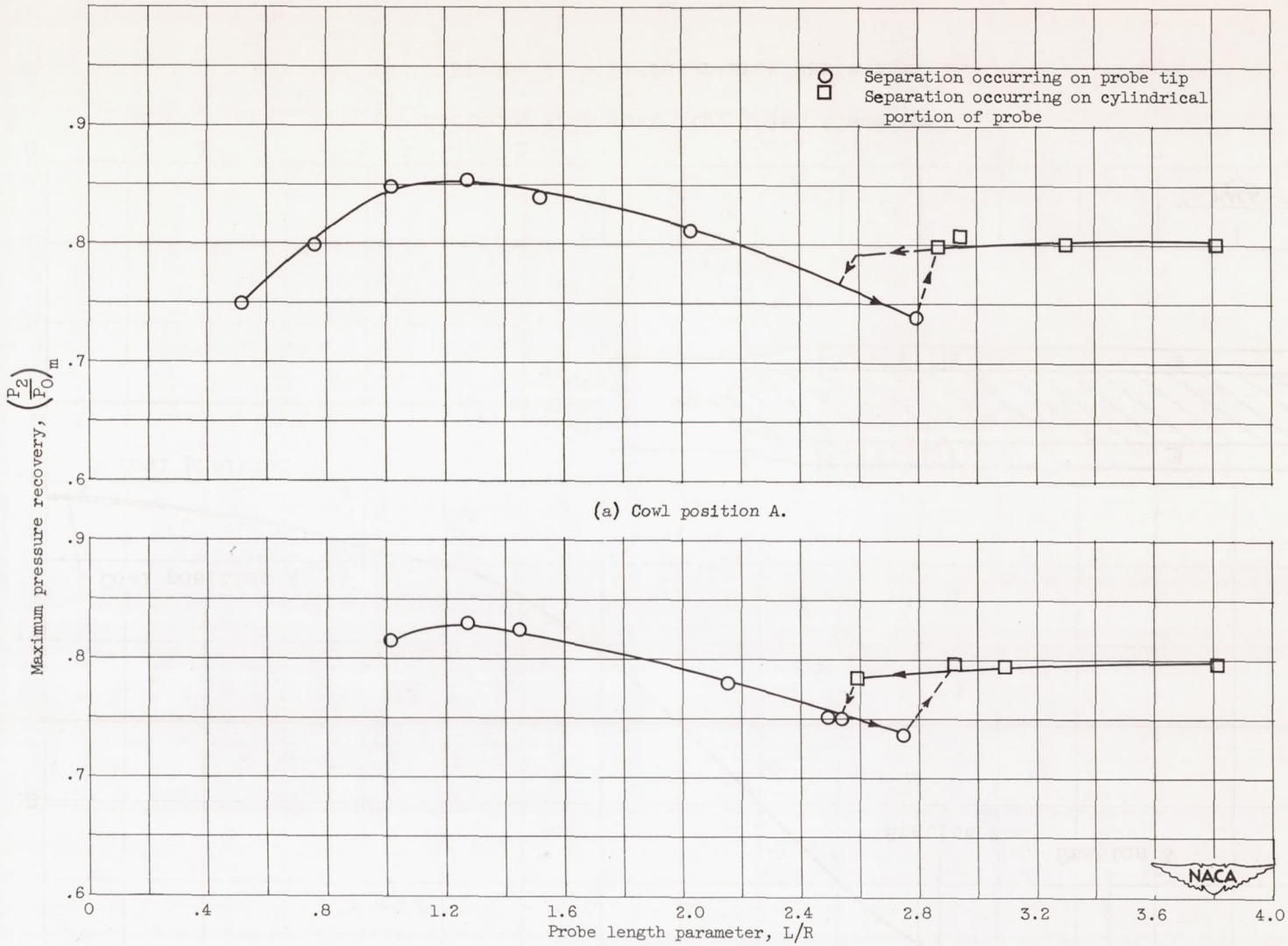

(a) Cowl position A.

(b) Cowl position B.

Figure 5. - Variation of maximum pressure recovery with probe length parameter. Free-stream Mach number, 2.0; angle of attack, 0°.

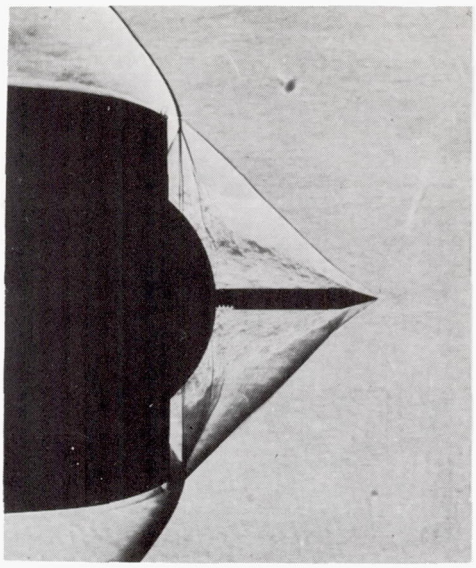

(a) Cowl position A; $L/R = 1.27$; $(P_2/P_0)_m = 0.85$.

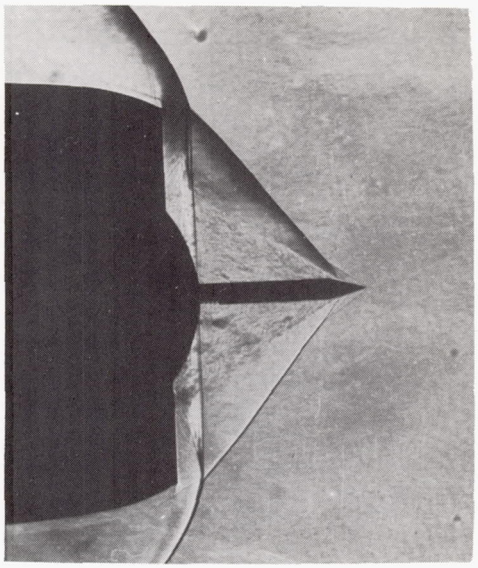

(b) Cowl position B; $L/R = 1.27$; $(P_2/P_0)_m = 0.83$.

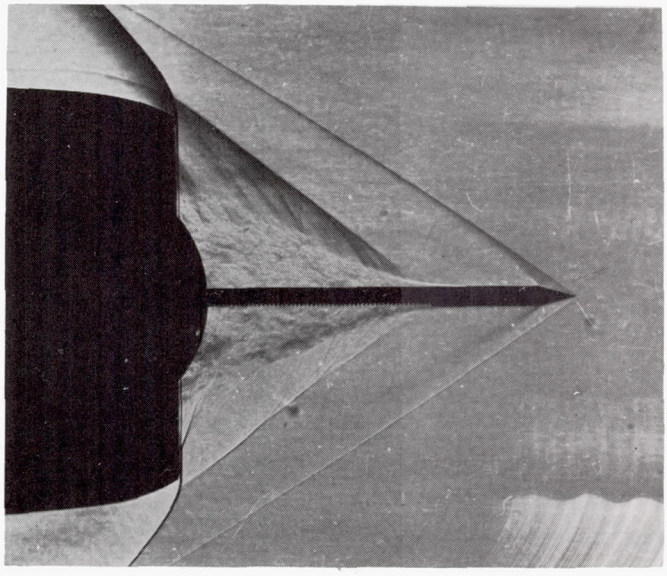

C-31124

(c) Cowl position B; $L/R = 2.92$; $(P_2/P_0)_m = 0.80$.

Figure 6. - Schlieren photographs at free-stream Mach number of 2.0 and zero angle of attack.

3B

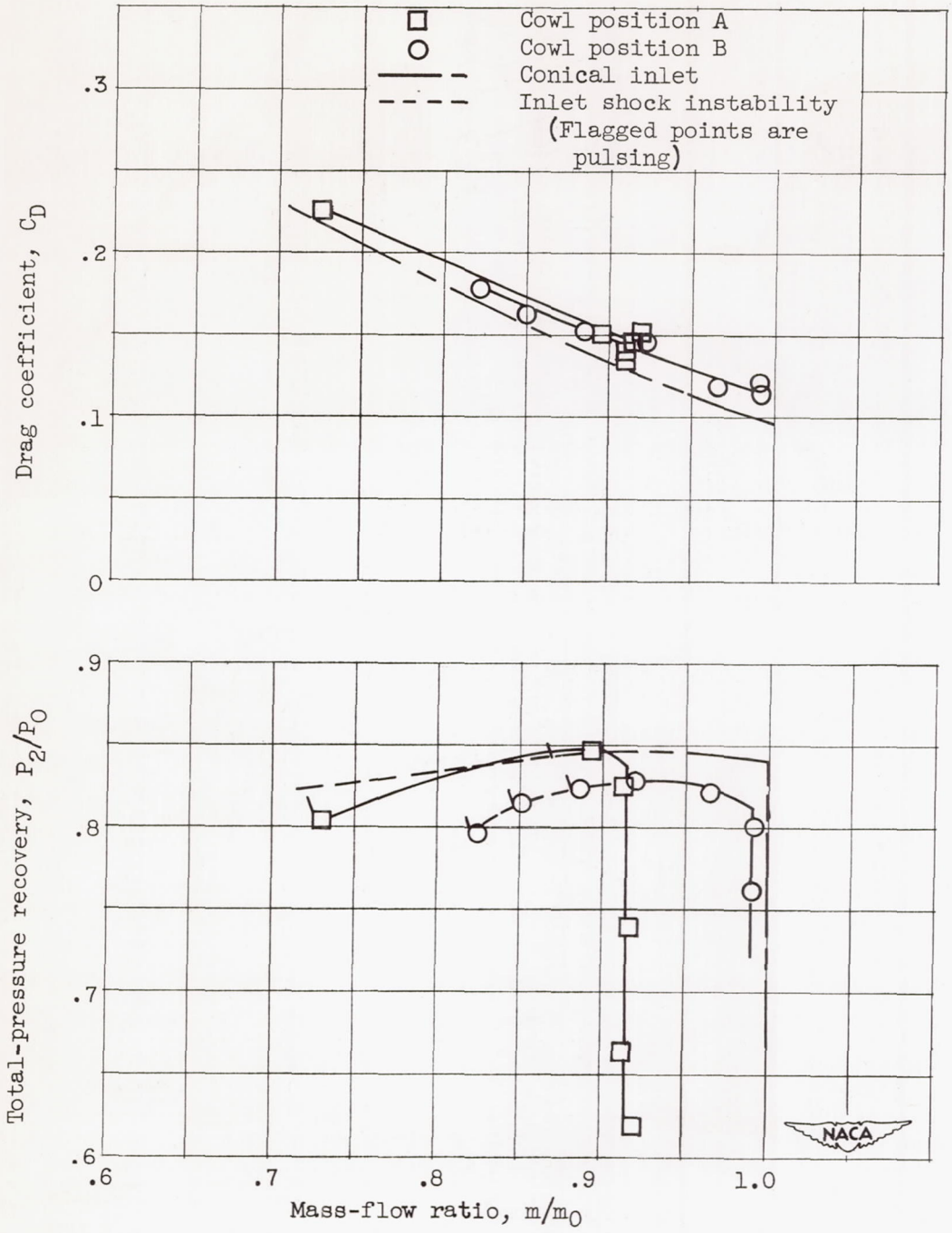

Figure 7. - Performance comparison for different cowl positions with comparable conical inlet at free-stream Mach number of 2.0 and zero angle of attack.

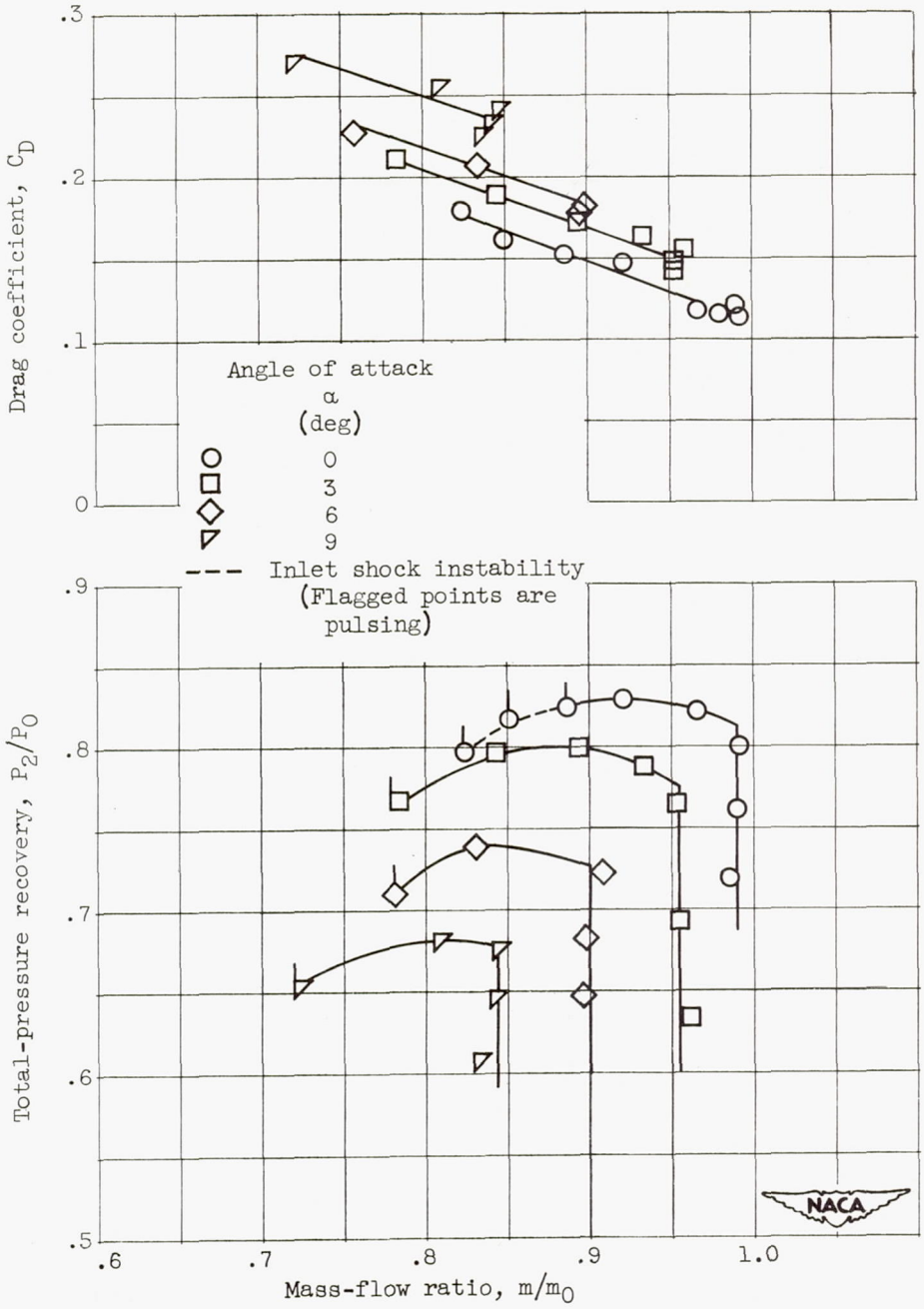

(a) Free-stream Mach number, 2.0.

Figure 8. - Performance of straight probe for cowl position B and probe length parameter of 1.27.

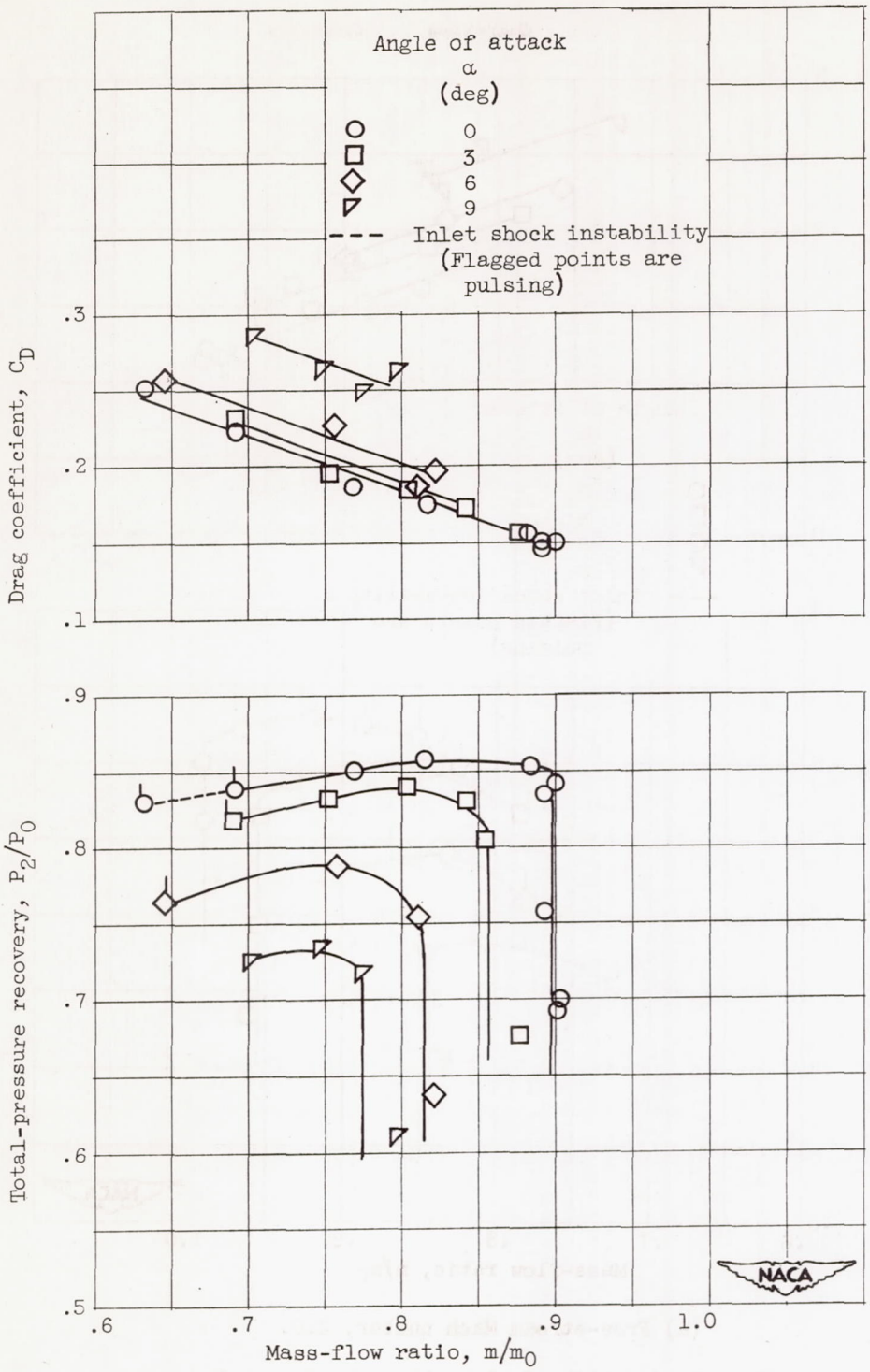

(b) Free-stream Mach number, 1.8.

Figure 8. - Continued. Performance of straight probe for cowl position B and probe length parameter of 1.27.

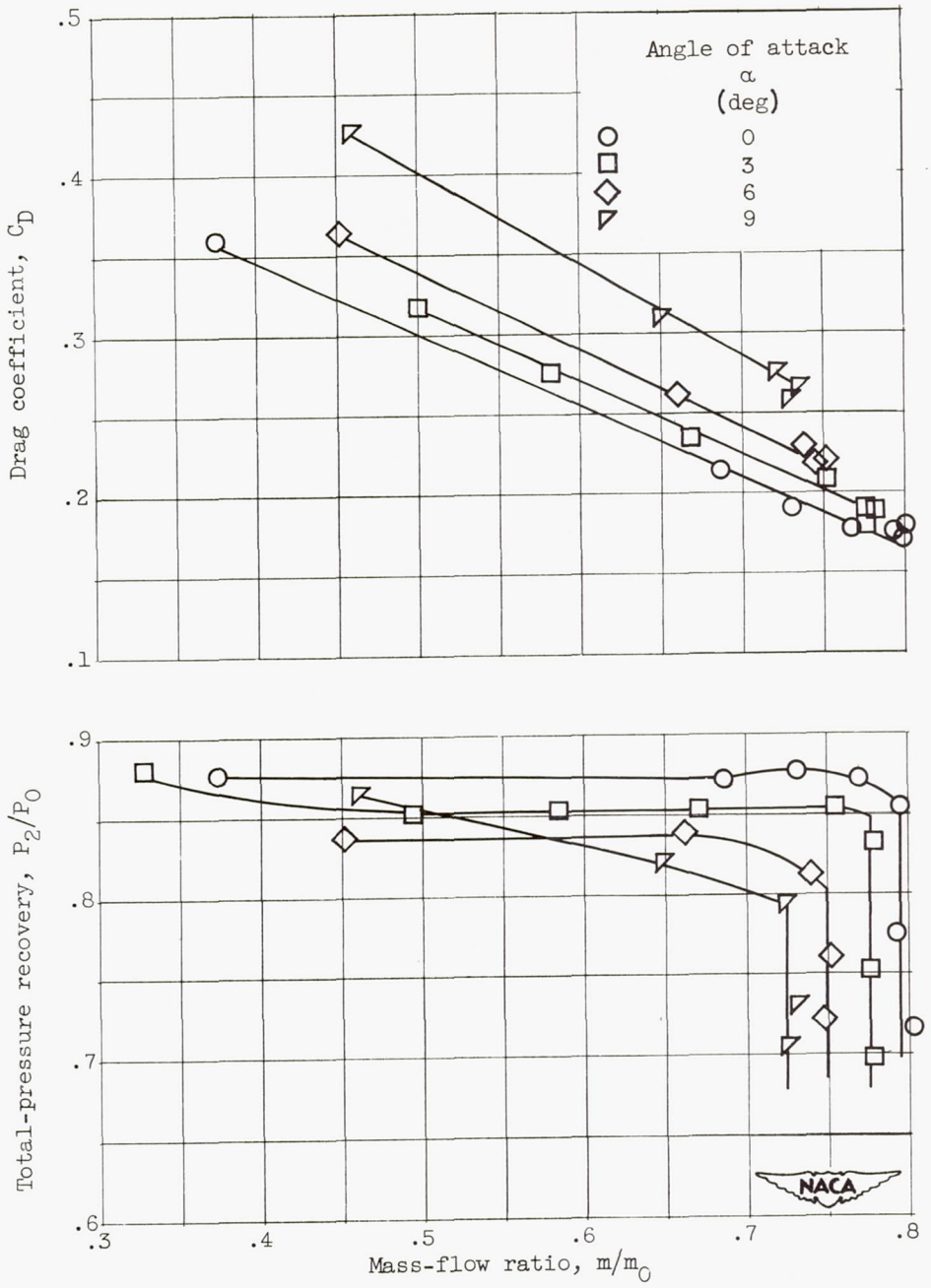

(c) Free-stream Mach number, 1.6.

Figure 8. - Concluded. Performance of straight probe for cowl position B and probe length parameter of 1.27.

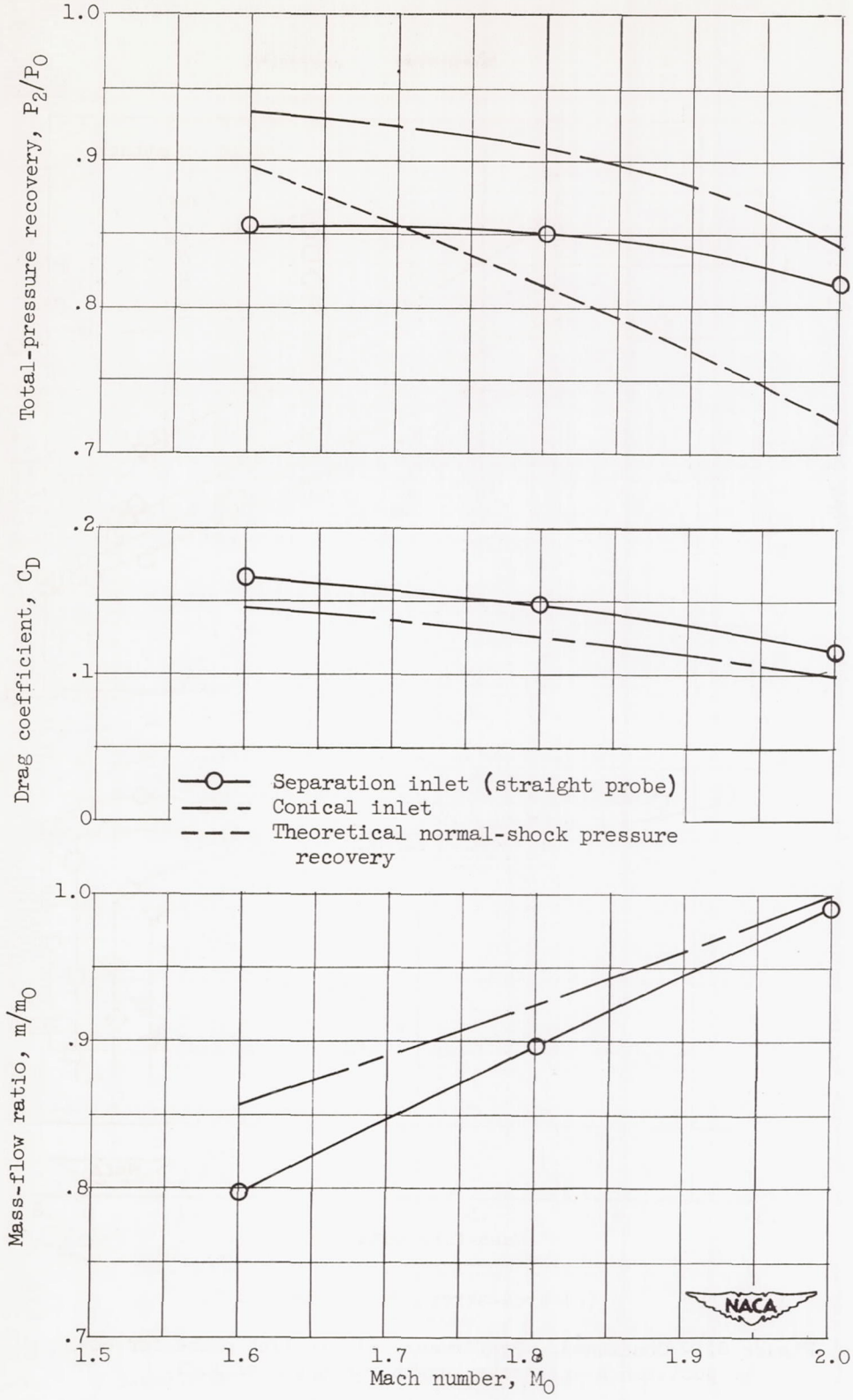

(a) Critical operation.

Figure 9. - Effect of Mach number on inlet performance at zero angle of attack.

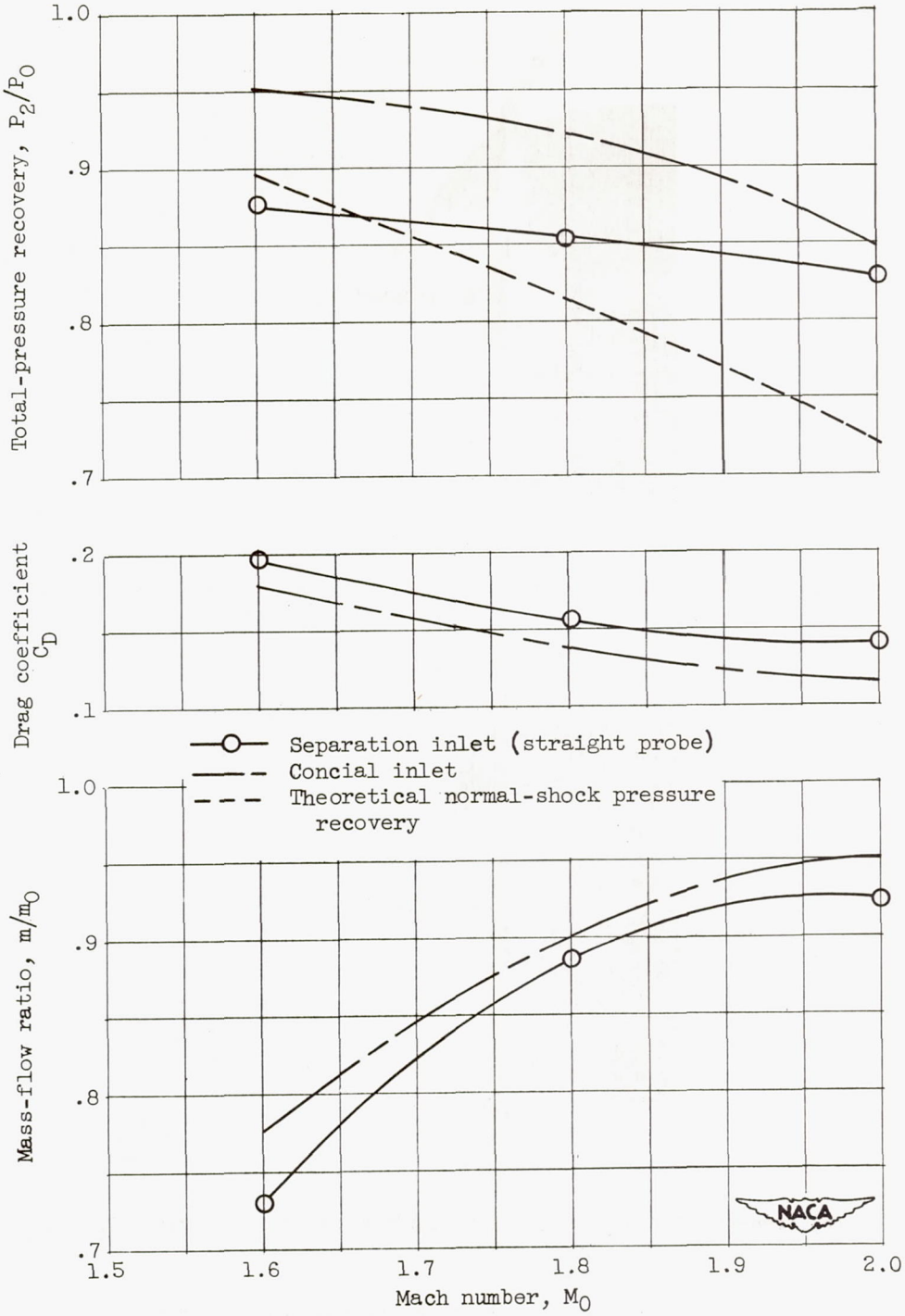

(b) Maximum-pressure-recovery operation.

Figure 9. - Concluded. Effect of Mach number on inlet performance at zero angle of attack.

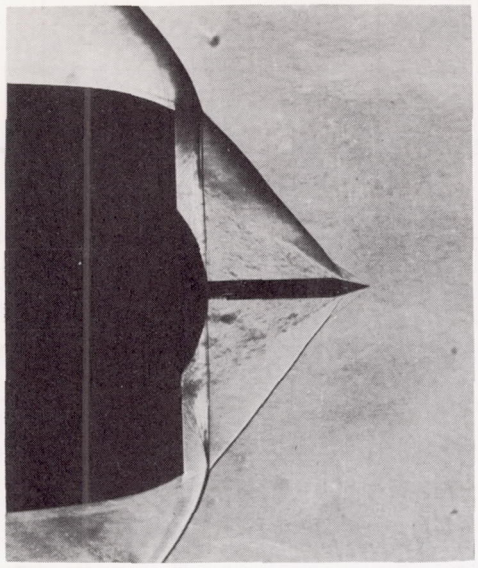

(a) Free-stream Mach number, 2.0; maximum pressure recovery, 0.83.

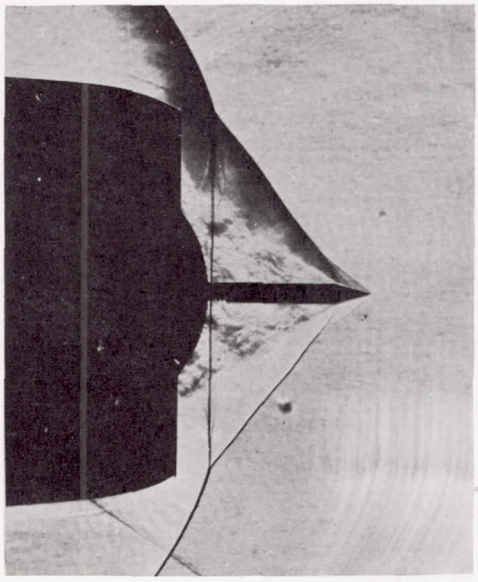

C-31125

(b) Free-stream Mach number, 1.8; maximum pressure recovery, 0.86.

Figure 10. - Schlieren photographs at zero angle of attack.

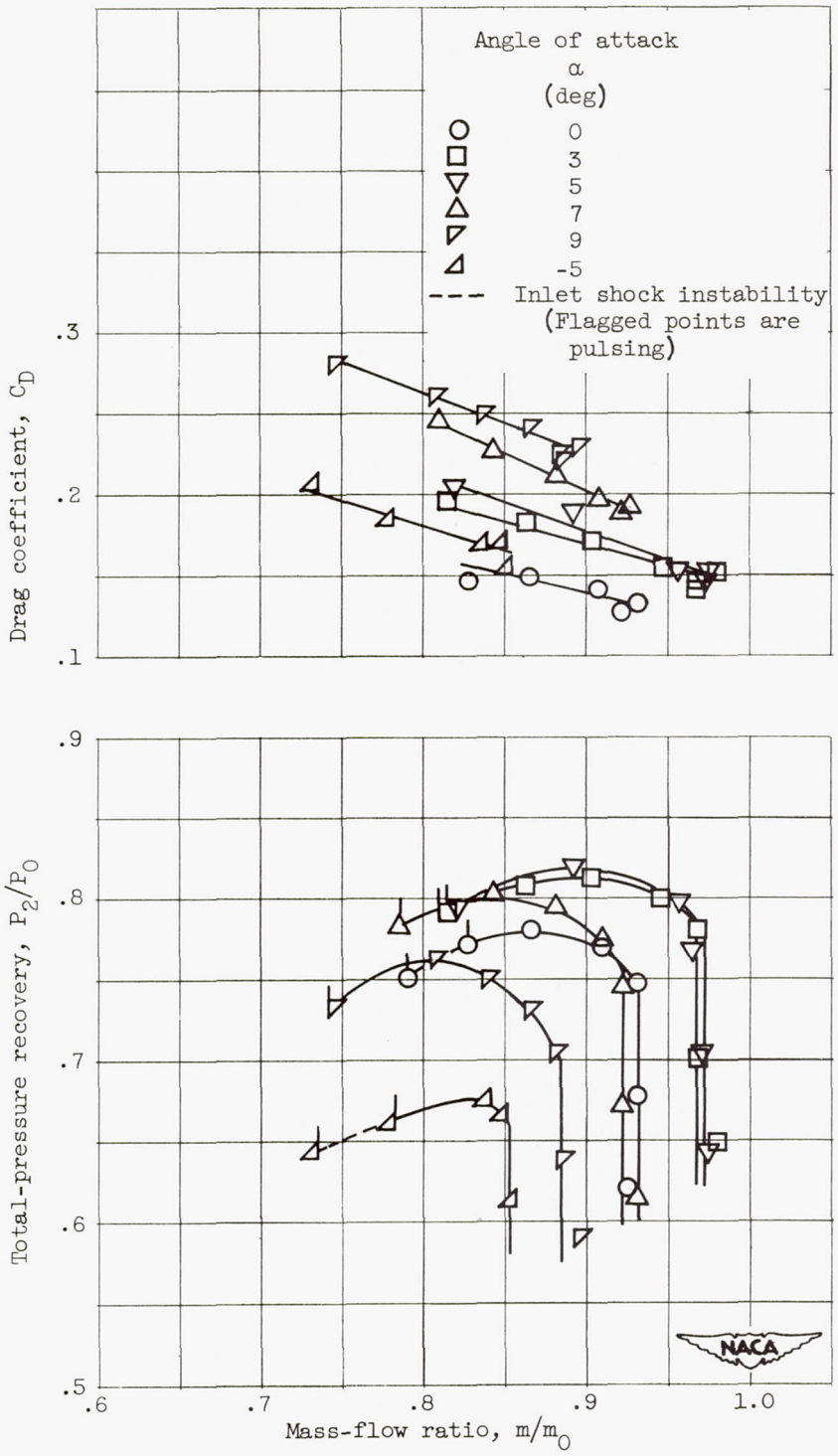

(a) Free-stream Mach number, 2.0.

Figure 11. - Performance of 5° offset probe for cowl position B and probe length parameter of 1.27.

4B

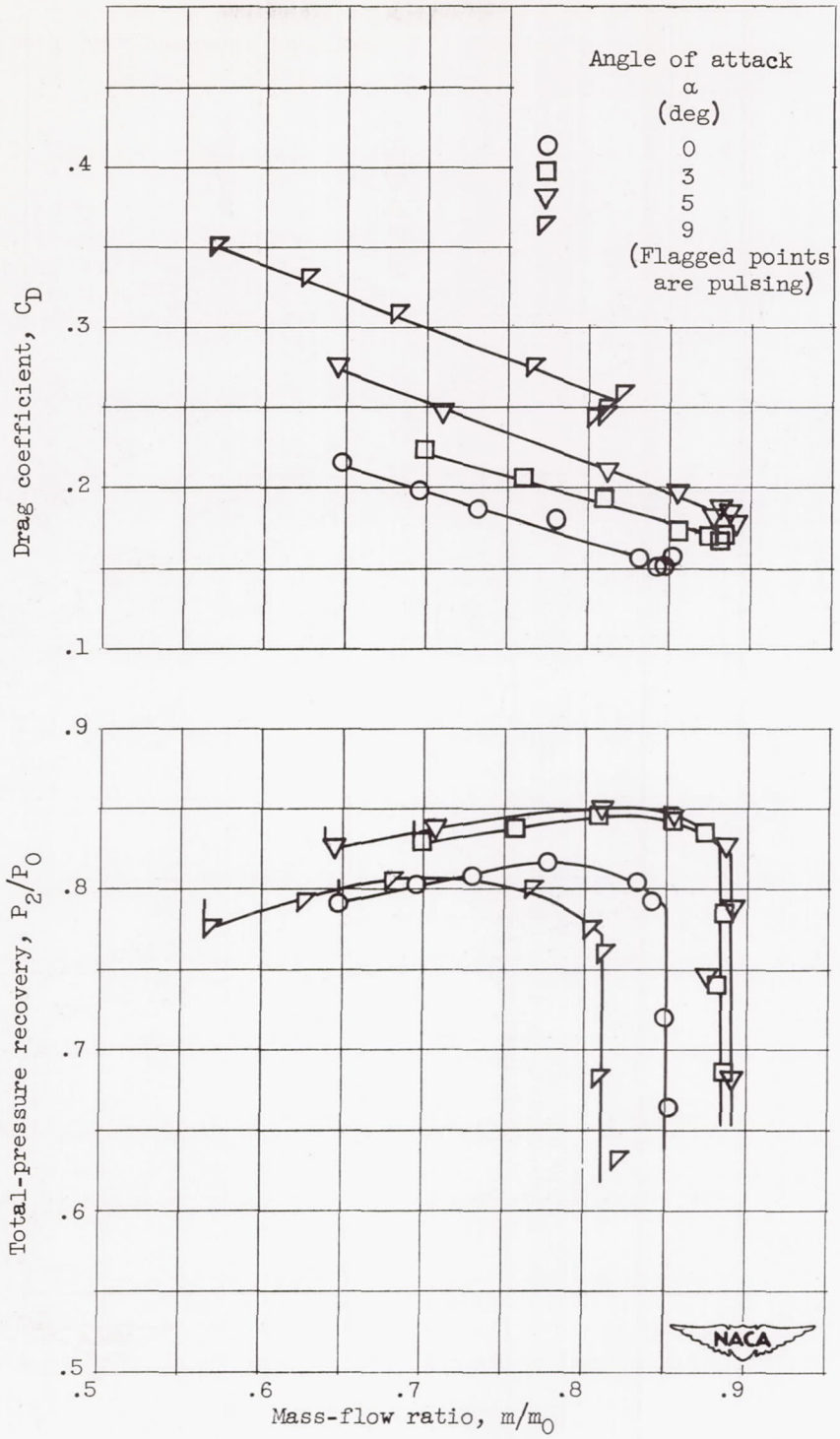

(b) Free-stream Mach number, 1.8.

Figure 11. - Continued. Performance of 5° offset probe for cowl position B and probe length parameter of 1.27.

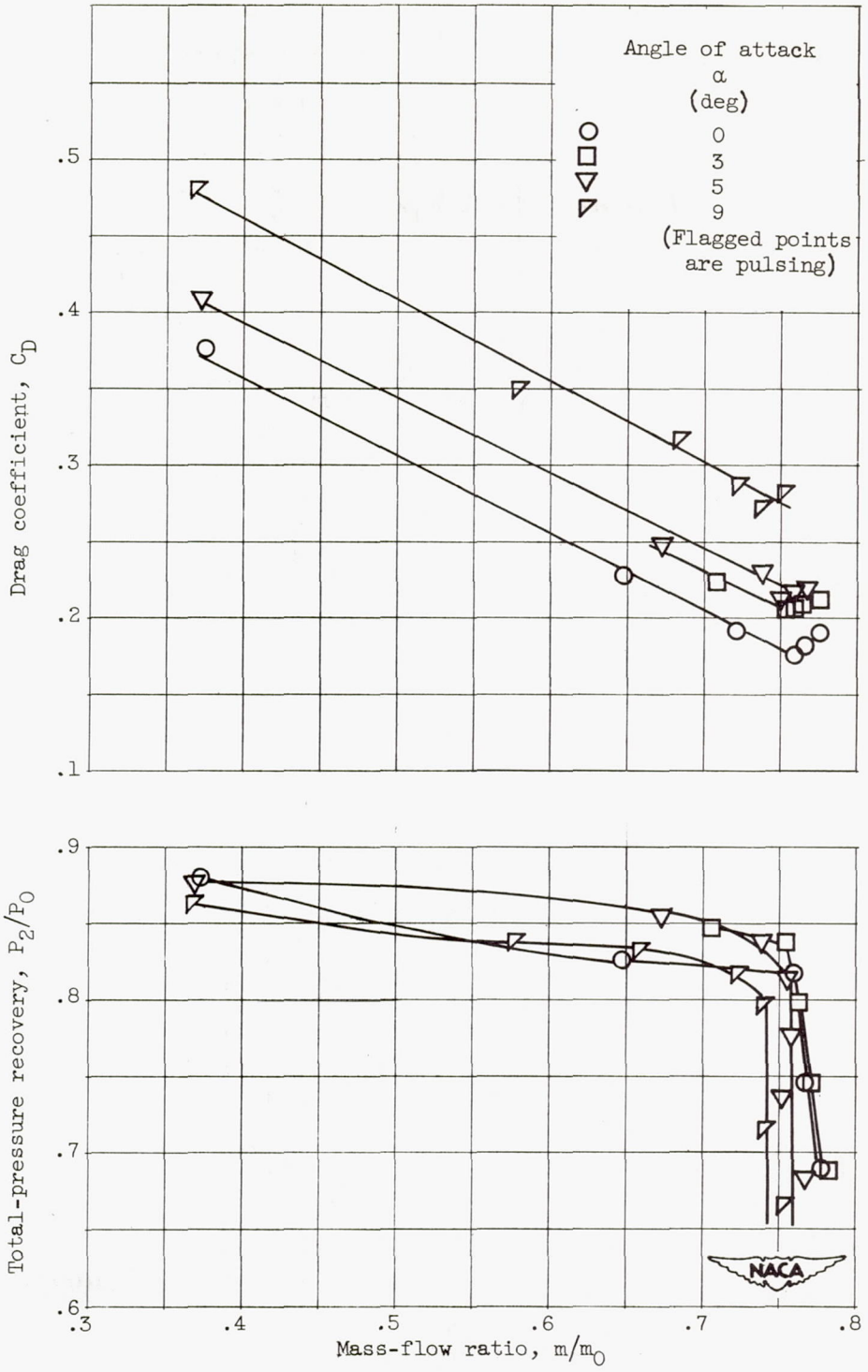

(c) Free-stream Mach number, 1.6.

Figure 11. - Concluded. Performance of 5° offset probe for cowl position B and probe length parameter of 1.27.

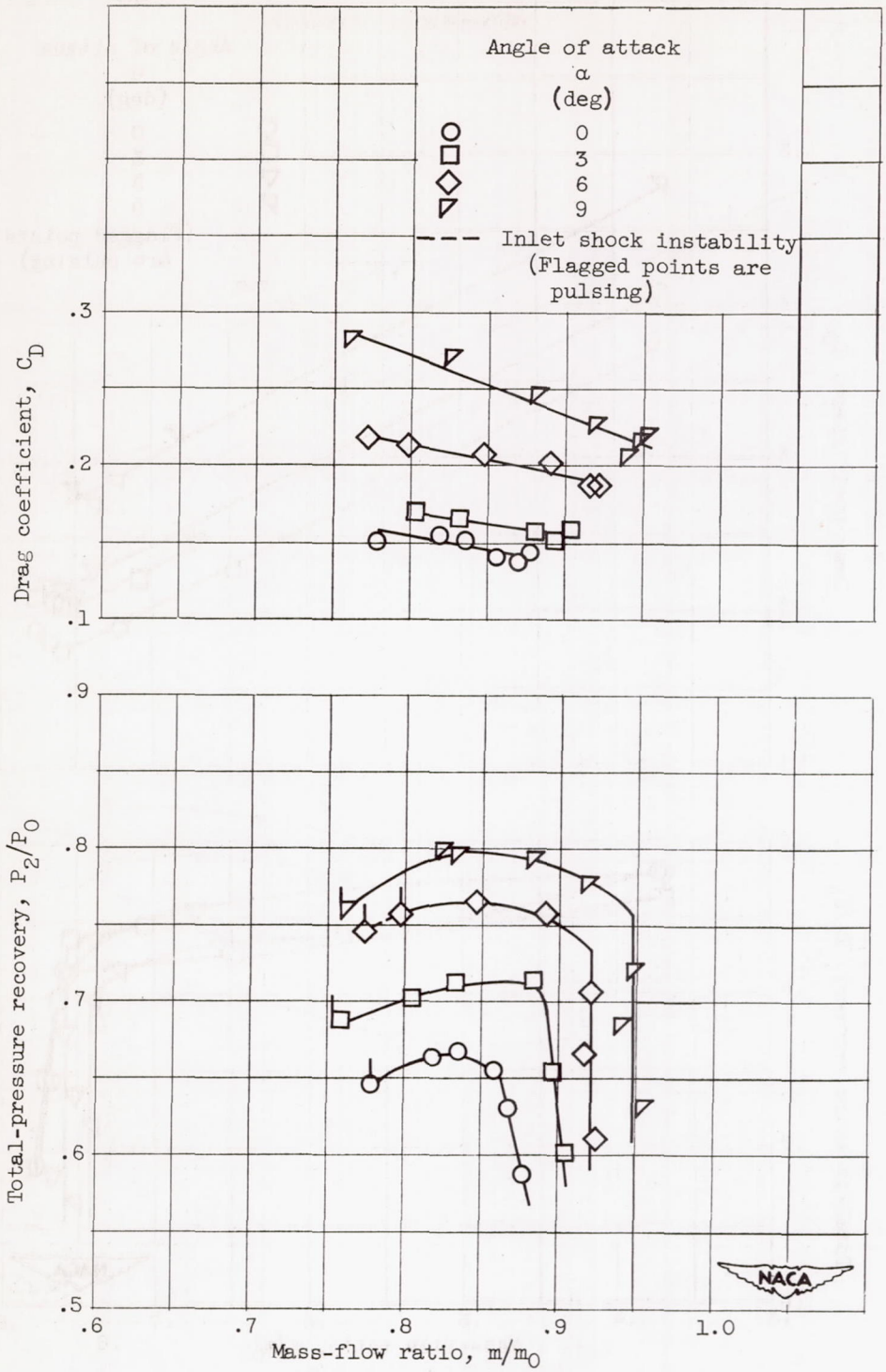

(a) Free-stream Mach number, 2.0.

Figure 12. - Performance of 10° offset probe for cowl position B and probe length parameter of 1.27.

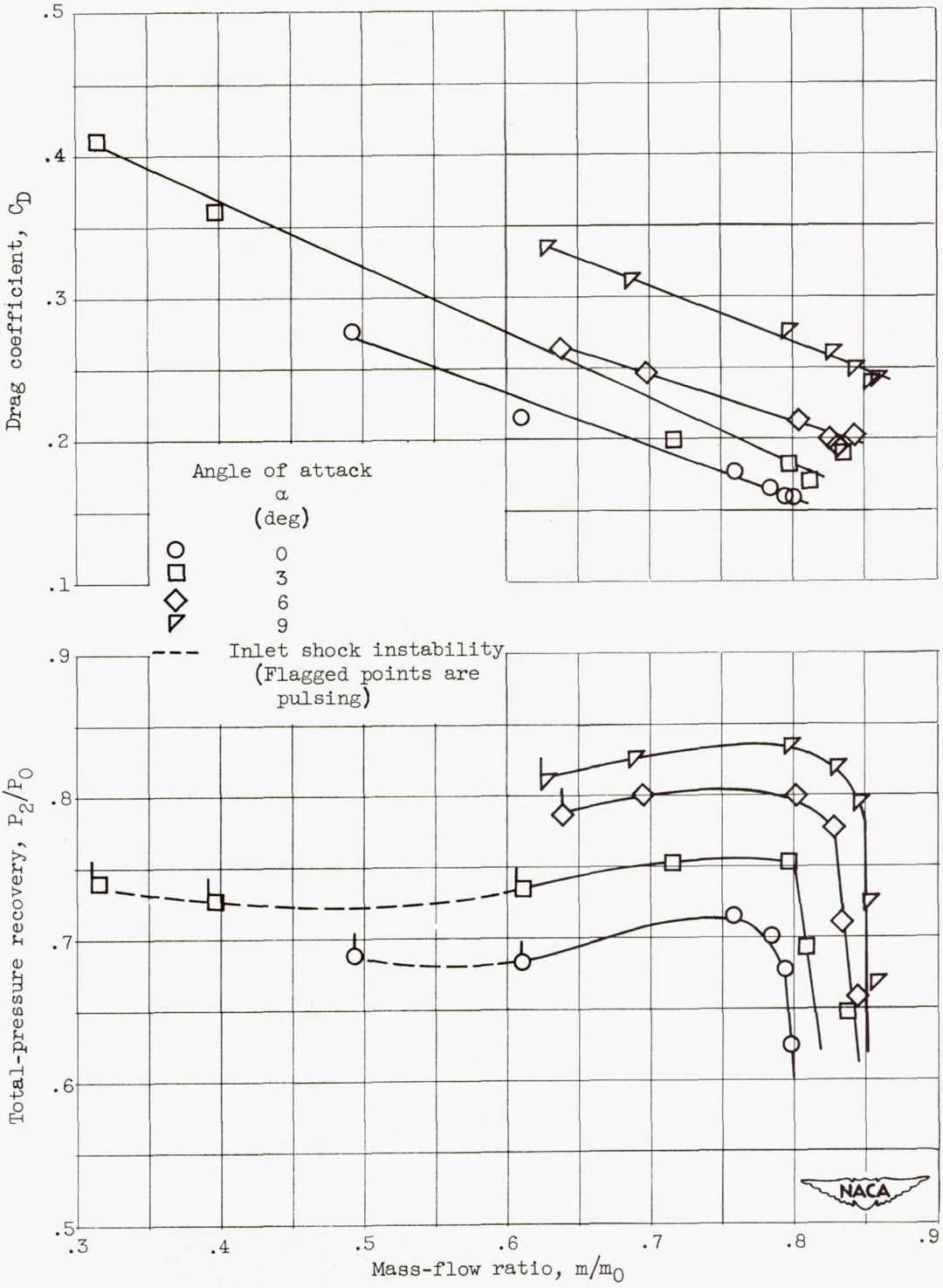

(b) Free-stream Mach number, 1.8.

Figure 12. - Continued. Performance of 10° offset probe for cowl position B and probe length parameter of 1.27.

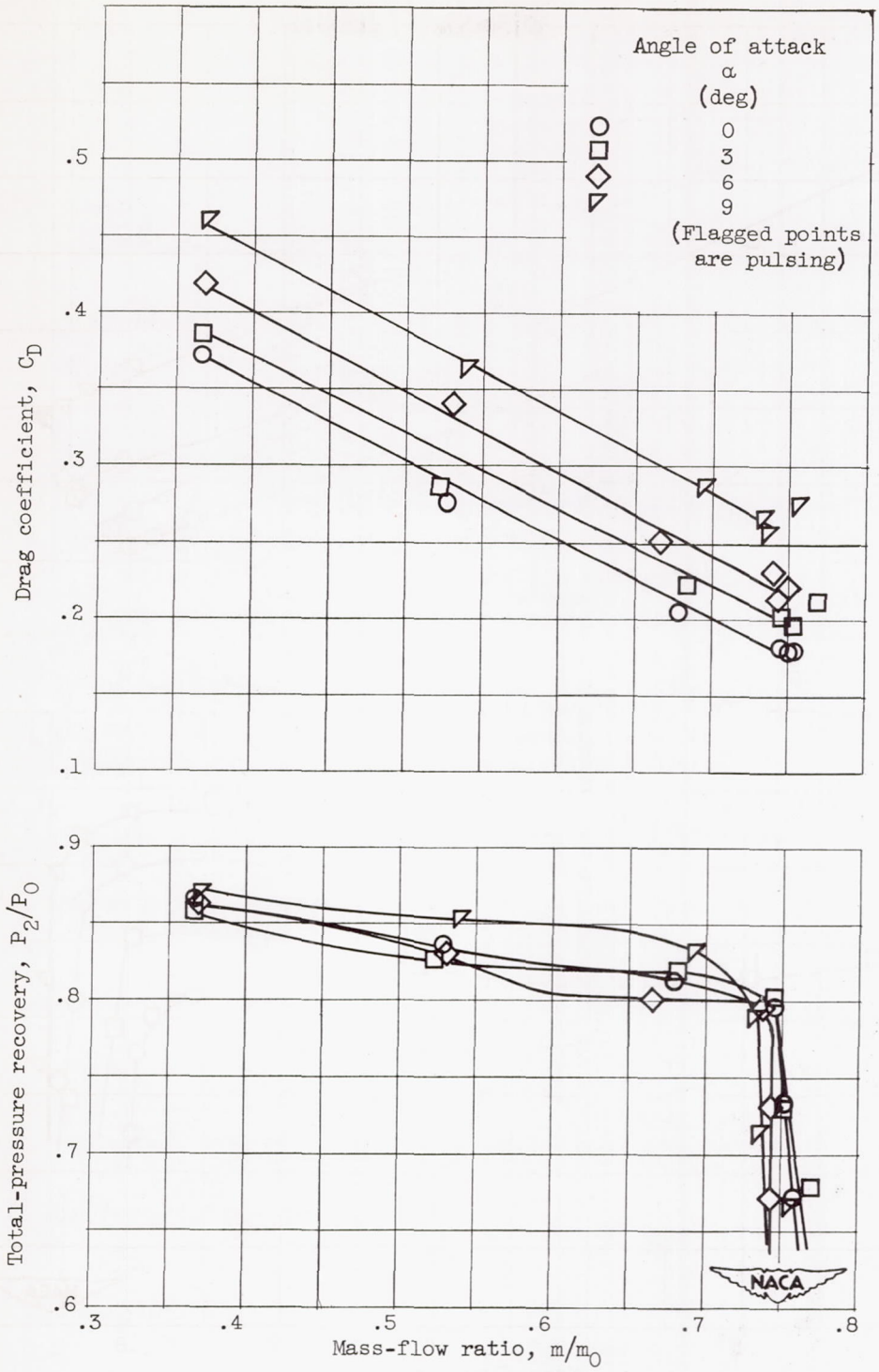

(c) Free-stream Mach number, 1.6.

Figure 12. - Concluded. Performance of 10° offset probe for cowl position B and probe length parameter of 1.27.

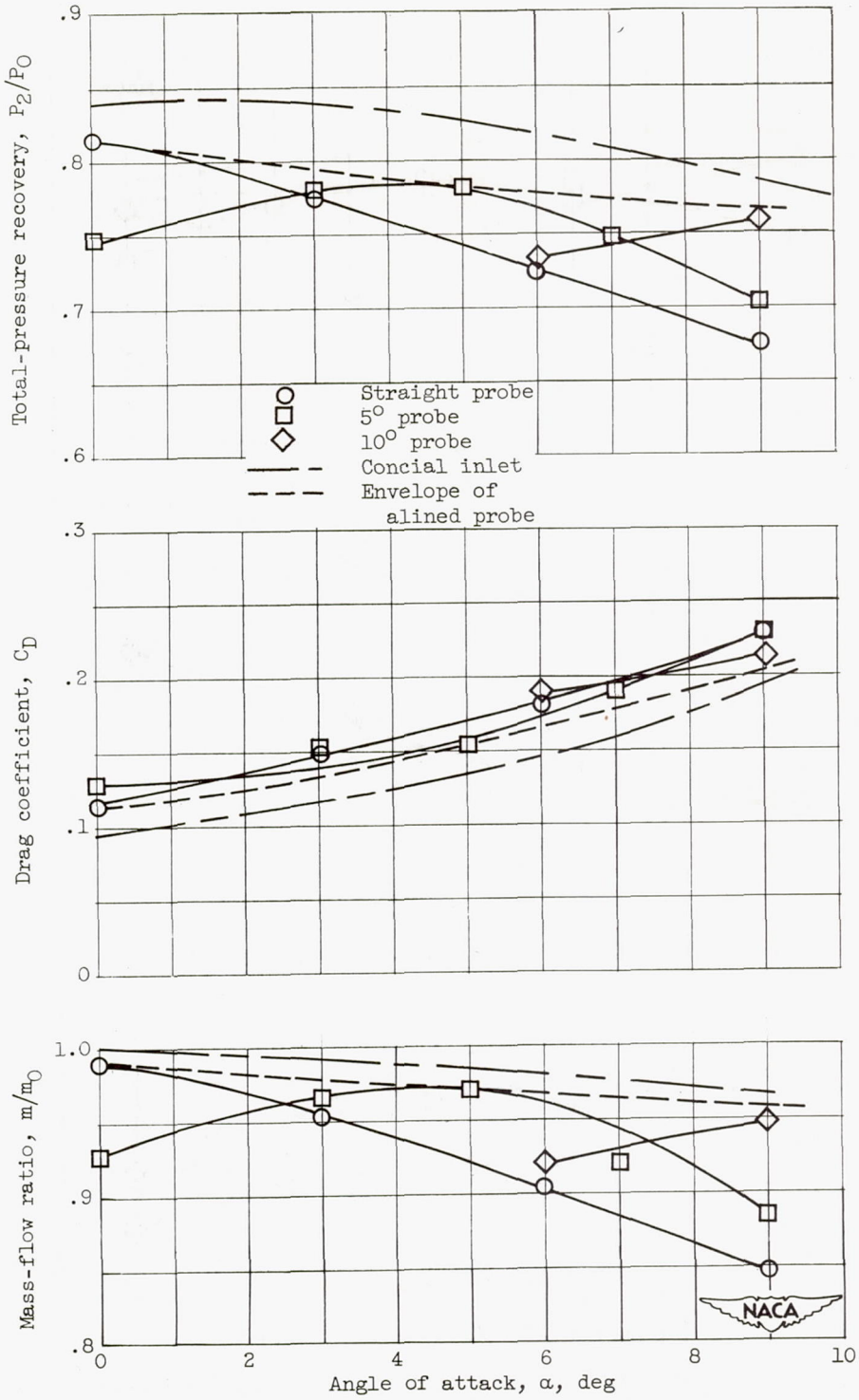

(a) Critical operation.

Figure 13. - Effect of angle of attack on inlet performance at free-stream Mach number of 2.0.

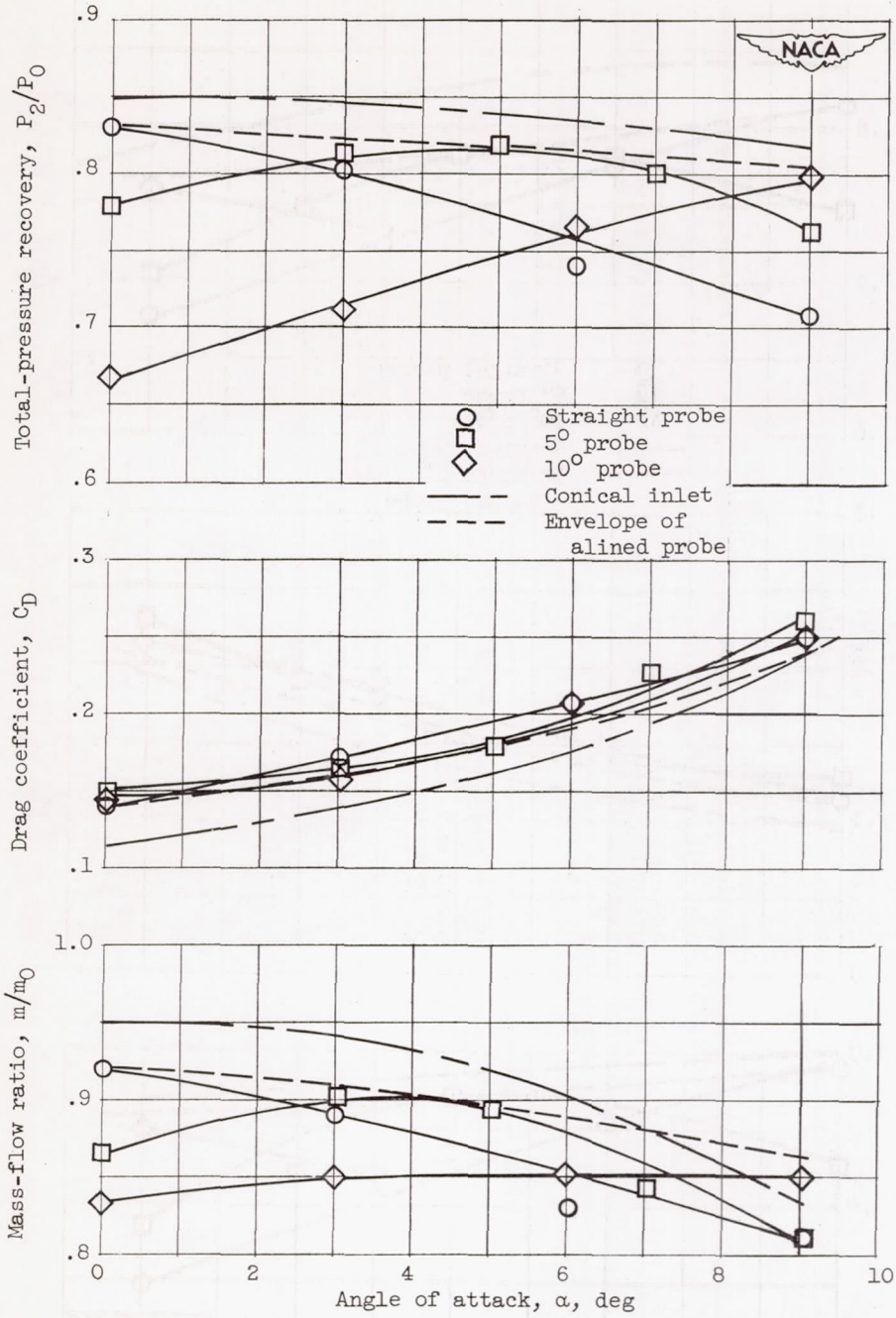

(b) Maximum-pressure-recovery operation.

Figure 13. - Concluded. Effect of angle of attack on inlet performance at free-stream Mach number of 2.0.

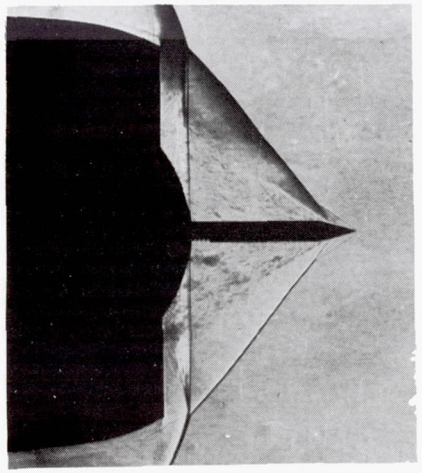

(a) Straight probe; $\alpha = 0^{\circ}$; $(P_2/P_0)_m = 0.83$.

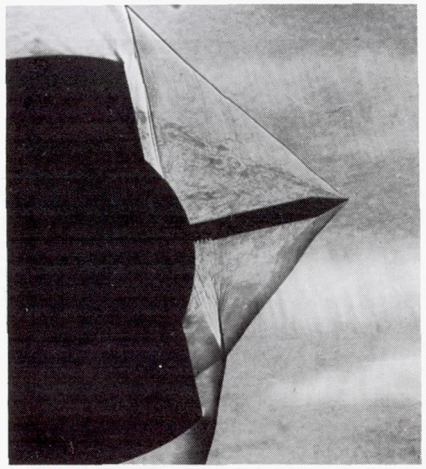

(b) Straight probe; $\alpha = 6^{\circ}$; $(P_2/P_0)_m = 0.74$.

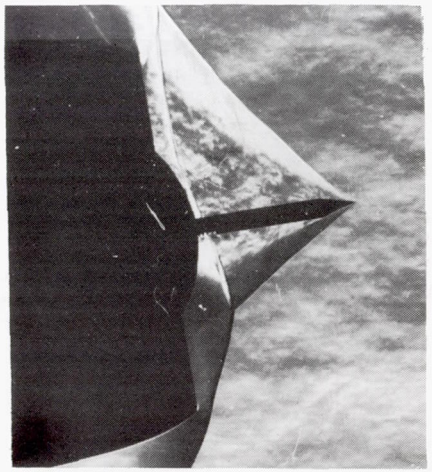

(c) Straight probe; $\alpha = 9^{\circ}$; $(P_2/P_0)_m = 0.68$.

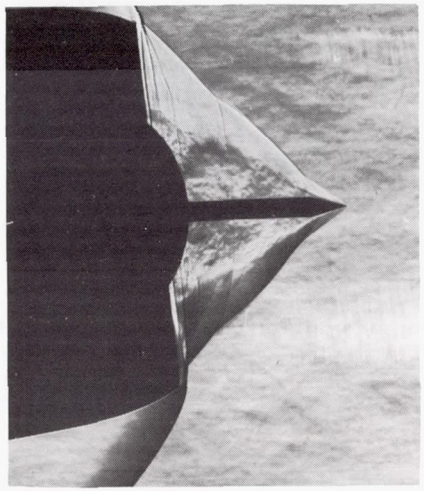

(d) 5° probe; $\alpha = 5^{\circ}$; $(P_2/P_0)_m = 0.82$.

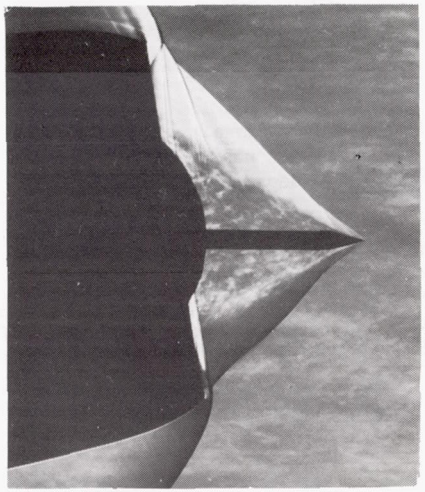

(e) 10° probe; $\alpha = 9^{\circ}$; $(P_2/P_0)_m = 0.80$.

Figure 14. - Schlieren photographs at free-stream Mach number of 2.0 for various angles of attack.

NACA
C-31126